Karipoth, P., Pullanchiyodan, A., Christou, A. and Dahiya, R. (2021) Graphite-based bioinspired piezoresistive soft strain sensors with performance optimized for low strain values. *ACS Applied Materials and Interfaces*, 13(51), pp. 61610-61619. (doi: 10.1021/acsami.1c14228)

There may be differences between this version and the published version. You are advised to consult the published version if you wish to cite from it.

http://eprints.gla.ac.uk/260108/

Deposited on 7 December 2021

Enlighten – Research publications by members of the University of Glasgow
http://eprints.gla.ac.uk

Graphite based Bioinspired Piezoresistive Soft Strain Sensor with Performance Optimized for Low Strain Values

*Prakash Karipoth, Abhilash Pullanchiyodan, Adamos Christou, and Ravinder Dahiya**

Bendable Electronics and Sensing Technologies (BEST) Group, James Watt School of Engineering, University of Glasgow, G12 8QQ, UK

E-mail: Ravinder.Dahiya@glasgow.ac.uk.

Keywords: strain sensor, piezoresistive, Velcro, bioinspiration, gauge factor

Abstract: This paper presents the custom-made graphite based piezoresistive strain sensor with gecko-foot inspired macroscopic features realized using a Velcro tape on Ecoflex substrate. The Velcro based design provides an inexpensive and easy approach for development of soft sensor with appreciable improvement in the performance even at low strain values. The sensor demonstrated excellent response (sensitivity ~16500%, gauge factor ~3800) for 24% linear strain. The fabricated device showed a high gauge factor (>100) even for very low strain values. The sensor has been extensively characterized with a view to potentially use in soft robotics application where high-performance is needed at lower strain values. It is observed that the piezoresistive behaviour of strain sensors is governed by several factors such as the supporting elastic medium,

architecture of the strain sensor, materials properties, strain rate and deformation sequence, and direction.

1. Introduction

Strain sensors with high sensitivity and reliable operation are needed in several applications related to flexible and stretchable electronics[1-4], wearable technology[5, 6], prosthetics[7, 8], structural health monitoring[9, 10], conventional robotics[2, 10, 11] as well as soft robotics[12-16]. Traditionally, the strain sensors integrated on various surfaces or structures, translate the mechanical deformations into electrical, optical or similar signals which are systematically processed to interpret the mechanical state of the system[17]. In this aspect, reported strain sensors are based on capacitive[18], piezoresistive[19], inductive[20], and optical[21] transduction mechanisms. Among these, piezoresistive sensors has been explored more due to their high sensitivity, easy fabrication, diverse choice of materials and designs, easy integration, conformability and deployability in diverse environments and applications[17, 22]. Various materials explored for conductive network in piezoresistive strain sensors include Ag nanowires[23], ZnO[24], conductive liquids[8, 25], carbon black[26], graphite[27], graphene[28], CNT[29], etc. Among these, carbon-based materials have been explored more, owing to their abundant availability, cost-effectiveness, tunable electrical properties, large operational window, dispersibility in variety of solvents and supporting matrix, and suitable mechanical features. To enhance the performance, several bioinspired designs have been adopted to design the strain sensor architecture, realize microscopic textured substrate, and the distribution of sensing material. Some of these approaches has been successful in improving the figures of merit[30-33], but their poor repeatability and realization using complex fabrication procedures limit their practicability.

A typical piezoresistive strain sensor involves a two- or three-dimensional network of conductive materials whose electrical conductivity is governed by the percolation pathway modulated by the degree of mechanical deformation. Several such sensors with stretchability of the order of several hundred percentage of linear strain have been reported with sensitivity ranging from <10 to the order of 1000[15, 17, 22, 34]. A vast majority of these highly stretchable sensors exhibit high performance metrics only when the linear strain is high and the key figures of merit such as sensitivity and gauge factor (GF) are significantly lower in the lower linear range of 0-20%[17, 19, 22]. As a result, the performance requirements for many applications[35] such as robotics, and wearables, where the maximum stretchability needed is often within 10 to 20% linear strain[36], are not met. For example, the stretchability of human skin is ~15%[37] and hence the applications mimicking human skin should have strain sensor showing excellent performance in this range of deformations. Considering this, it is important to develop reliable and robust strain sensors with high sensitivity, and fast response even at lower strain rate. "A few recent reports on crack based piezoresistive strain sensors have shown high sensitivity and gauge factor.[38] However, a major drawback of crack-based strain sensors is that the generation and propagation of cracks is random or unpredictable. In most cases, they require additional fabrication steps to generate cracks and their characteristics (which govern the sensing performance) cannot be predefined. The geometrical optimization of the state-of-art crack-based strain sensors is not readily feasible. As a result, they are less reproducible. Recently, researchers[39] have also demonstrated strain sensors with high gauge factor and stability. However, the tedious fabrication steps needed to optimize the geometrical designs, and tough conductive fibres, are incompatible with conductive ink-based approaches."

With high sensitivity at lower strain values itself, the strain sensor presented here addresses this need. Various parameters that influence the piezoresistive strain sensing mechanism are studied to interpret quantitatively and qualitatively the complex constellations and configuration of mechanical systems. This is important as often the output of piezoresistive strain sensor is presented in terms of the magnitude of deformation (as a function of strain percentage) and there is limited or no information provided about the mechanical deformation pathway, stable equilibrium states[40], influence of strain rate[41], and viscoelastic relaxation[42]. These are important factors, as with current practice, of associating the output of piezoresistive strain sensor with a calibrated value of corresponding linear strain, little or no information could be drawn to distinguish the responses originating from bending or stretching. Since the sensing mechanism is governed by electrical percolation[43], the orientation and reorganization of the conductive network plays an important role in the interpretation of the mechanical state. The sensor response can also depend on the strain rate, viscoelastic relaxation, and hysteresis[44] and hence the detailed study can help to properly attribute the response to various parameters at play. Such detailed analysis could improve the understanding about the working of strain sensors and help unravel the complex dynamics of the mechanical systems.

Considering the various aspects discussed above, the design and characterization of a e custom-made graphite paste based piezoresistive strain sensor is presented here. This piezoresistive sensor follows a simple design having macroscopic features, realized with a Velcro tape on Ecoflex substrate to enhance the performance. The Velcro tape allowed us to develop substrate with the macroscopic features inspired from gecko foot. The features are then filled with custom-made graphite paste to obtain the sensor that can provide high sensitivity at lower strain values itself. Among various substrates explored for flexible and stretchable strain sensors, the silicone

elastomers, polyurethane, fabric, plastic, paper, or Kapton are most common. However, only limited reports on carbon based strain sensors on these substrates have demonstrated appreciable sensitivity and performance in the sensing range of 0-20 % linear strain[17, 22]. The strain sensor is studied for its strain sensing characteristics and various factors influencing the sensor responses.

2. Results and Discussion

2.1 Design and fabrication of Velcro enabled strain sensor

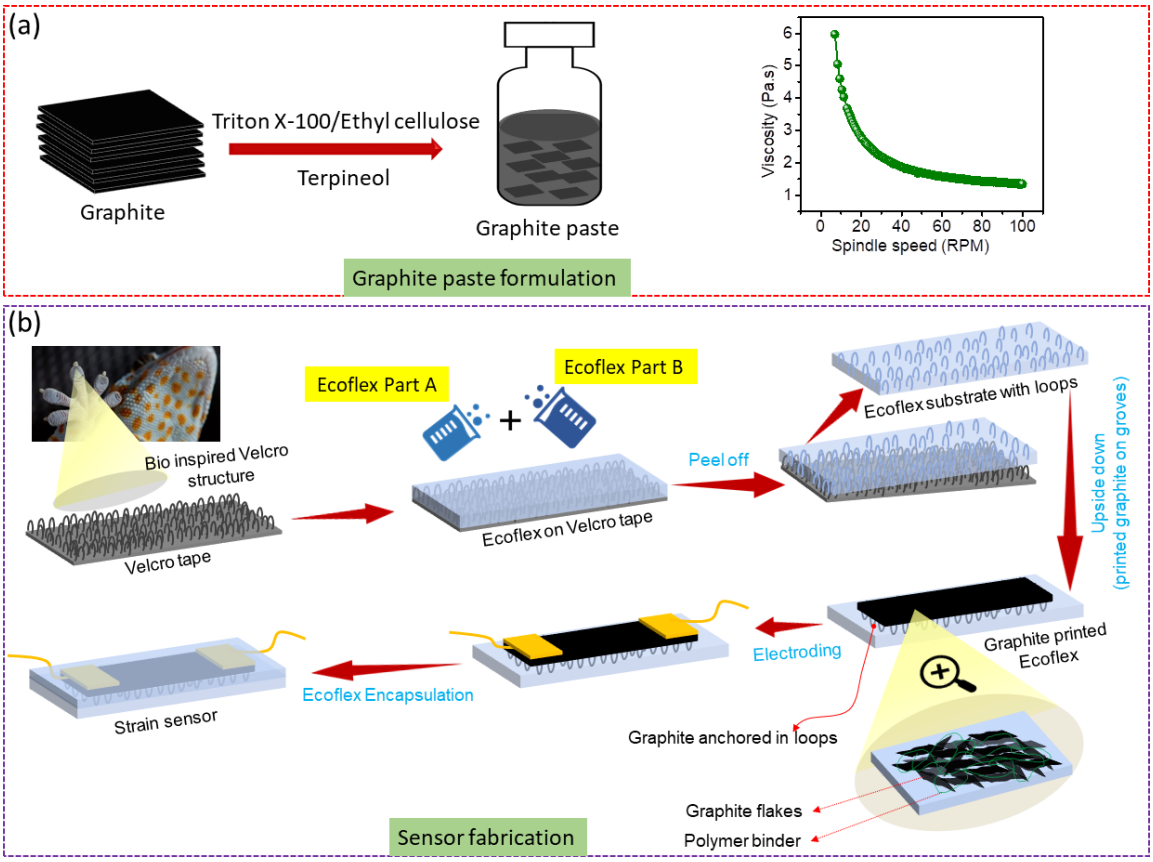

Figure. 1 (a) The schematic representation of the formation of graphite composite with ethyl cellulose and variation of viscosity with applied spindle speed (b) Fabrication steps of the strain sensor with graphite paste and Ecoflex.

The elastomeric substrate of the strain sensor was designed (see Figure 1) to have a Velcro hook structured micropores resembling naturally inspired designs[45] such as the pattern on gecko

foot. The detailed fabrication procedure is given in Experimental Methods Section. The motivation of utilizing the Velcro hook structures is based on several considerations: Firstly, the patterned pore structure distribution can enhance the mechanical roughness of otherwise smooth Ecoflex elastomer layer and thereby facilitate better adhesion between the graphite sensing layer and the elastomeric layer. Further, the Velcro-hook shaped micro pores serve as the anchoring points for the graphite layers mediated by the ethyl cellulose binder. These anchor points serve as the nodes about which the percolation paths for the electrical conduction can vary systematically with respect to the dimensional changes of the elastomer by external mechanical strains. In complex geometrical conductive networks, the strain sensing behavior is majorly governed by conductive tunnelling effect, in which tunnel nodes play a crucial role in modulating the resistance variation during structural deformations[46]. The study also showed that a 3D segregated spatially dependent network can provide reliable performance as compared to randomized and less correlated network in which node distribution are quite fragile. Apparently, in our work, the conductive material graphite having the inherent layered structure are known to exhibits shear properties. Hence, in a case where graphite conductive network is applied on a smooth elastomeric surface, graphite may slightly dislocate from their equilibrium distribution and hence are less likely to form high degree of correlated recoverable network and conducting nodes. In our followed approach of replica molding using Velcro tape, the Velcro features are engraved as surface texture in the form of correlated of distribution tiny pits on Ecoflex surface as represented in Fig. 1 (b). When the graphite paste is applied on the Velcro modified surface, the graphite network fills the pits as well as forms a continuous conducting distribution over the sensor region (see supporting information Figure S3). Thus, graphite trapped in the tiny Velcro pits serves as anchoring points or conductive nodes facilitating more spatially dependent and recoverable conductive network of graphite as

compared to a conductive network on a smooth elastomeric surface (see supplementary Figure S2. (b)). The role of anchored interconnection of conductive fillers for enhanced electrical conductivity is also validated by Zhu et al., [47] by utilizing predesigned hemisphere array of pits to distribute copper and carbon particles. In another reported work[48] on strain sensor with silver nanowire (AgNWs) in polyurethane (PU) matrix, it was reported that more the proportion of AgNWs tightly embedded in PU, the minimum will be the dislocation of AgNW layer during deformation. This has been attributed as an anchoring effect of the embedded structure facilitating the AgNW networks with a deformation identical to that of the PU matrix. Thus based on the literatures and our approach with Velcro enabled features, strain sensors with anchored conductive network possess comparatively higher degree of recoverable deformation of the network which is a significant for better durability, reliability and sensitivity as compared to loosely distributed conductive networks.[48]

The adopted replica molding of periodic hook structures in the commercial Velcro tape is an easy approach to obtain millimeter scale biomimetic features. Possibly similar macroscopic features could also be realized with standard microfabrication techniques or chemical bottom-up approaches, but this will involve complex and tedious process steps. In the case of gecko foot, it utilizes Vander walls forces and to achieve that, nanoscale or micron size features are required and may need sophisticated fabrication procedure to replicate. Hence, we have attempted to use commercial Velcro tapes with macroscopic features which can provide the gecko like effect in terms of surface modification with rough rubbery features of an otherwise smooth elastomeric substrate, but not on dimension scales or underlying principle.

2.2 Characterization and analysis of the strain sensor

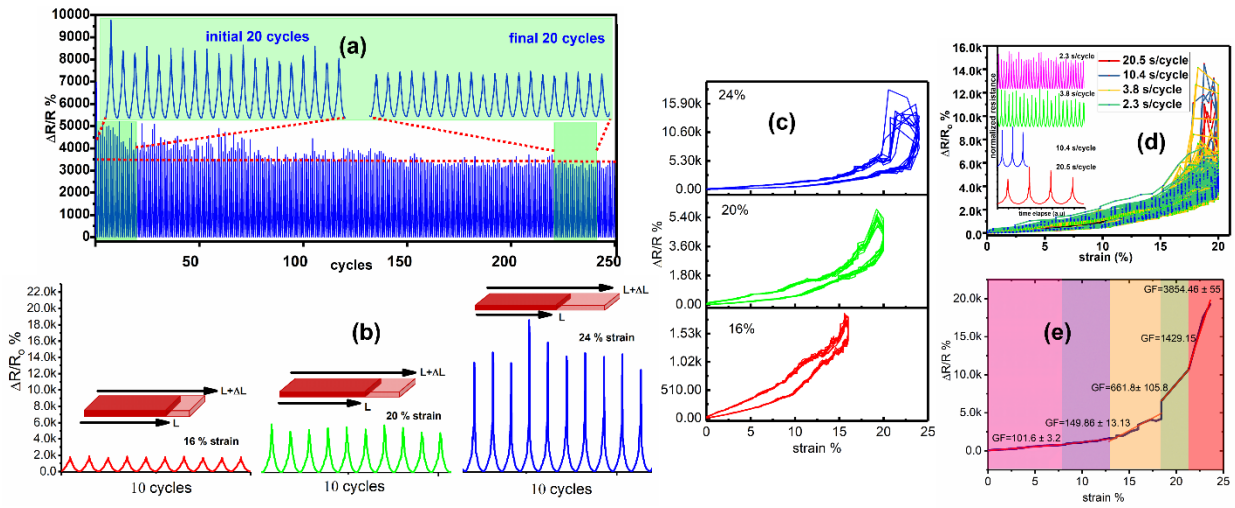

Figure. 2. Strain sensor performance (a) Dynamic strain response resistance variations of the fabricated strain sensor measured for 250 continuous cycles for 20% linear strain (b) Piezoresistive response and (c) hysteresis behaviour of the sensor for 16%, 20% and 24% linear strain, (d) Piezoresistive response of the sensor for 20% linear strain for varying strain rate (e) gauge factor.

Figure 2 (a) shows the dynamic response ($\Delta R/R_o$) of the fabricated strain sensor for 250 continuous cycles at 20% linear strain and a strain rate of 8.66%/s (2.31 s for 1 cycle). The details of sensor characterization arrangement are described in experimental section. The sensor exhibited quick, and sharp resistance variation in response to the time varying applied linear strain. The very high (~5000%) sensitivity ($\Delta R/R_o$%) observed for 20% of strain is shown in Figure 2(a). The variation of resistance towards the first (~1st-20th cycle) and last 20 (221st – 24th cycle) strain cycles (inset of the Figure 2(a)) show a fairly stable and consistent performance of the sensor. The stabilization of maximum $\Delta R/R_o$ after slight random fluctuations during initial few cycles indicates the improvement of elastic coupling between the sensing layer and the elastomer with successive cycles. From literatures, it is evident that during cyclic measurements of stretchable piezoresistive strain sensors on elastomers, initial drift or amplitude variations are probable and with the

successive cycles, the response will stabilize. This could arise from various factors dependent on both the elastomeric as well as conductive network behaviors. Hysteresis, material stress relaxation,[49] cyclic stress softening,[50] initial formation and propagation of microcracks in conductive network and temperature changes, all may contribute to drift of the sensor signal under a constant strain. Hence, initial few cycles, even when the cyclic measurements conditions remain constant, the sensing network and the elastomeric network may be less perfectly coupled elastically. But with successive cycles, the sensing layer and elastomer will be better coupled to each other. Here, during the initial cycles, the deformation of conductive graphite layer may not be perfectly identical with the deformation of the elastomer which synchronizes with successive cycles over time. Figure 2(b) depicts the stretch-strain cycle responses of the fabricated sensor linearly deformed to different values of maximum strain. The $\Delta R/R_o$ increases gradually for a lower strain valued (from 16% to 20%), but a sharp increase in resistance was observed after certain values (e.g., 24%). The sensor showed a mean relative resistance change of 2000%, 5000% and 16500% for 16%, 20% and 24% linear strain, respectively. The low hysteresis is observed during the stretch-release cycle (Figure 2(c)) and it is negligible for lower strain values as evident from the smaller enclosed area within the loop[51,52]. Hysteresis behavior is common during loading-unloading cycle in piezoresistive sensors[44,52]. This is governed by the percolation mechanisms[53] and its origin is attributed to the microstructure features - in present case, it is the asymmetric behaviour of graphite layers as a result of reorientation, sliding and buckling. The absolute area enclosed in the hysteresis for representative cycle was found to be approximately 3686, 14242, and 39883 calculated from Figure 2(c) for 16 %, 20 % and 24 % strain respectively. Even though it could be inferred that hysteresis is higher for higher applied strain, no quantitative conclusions could be arrived from the available hysteresis behaviour since the hysteresis analysis with respect

to resistance variation is not very reliable as it slightly varies with successive cycles attributed to the inherent origin or piezoresistance governed by percolation mechanism. So, model based hysteresis calculations or experimental measurements determining the stress-strain dependence are more quantitative assessment of hysteresis in viscoelastic elastomers. During the load-unload cycle, the mean-free path for the electric conduction shifts because of reorientation, and sliding. In any case, the sensor restores its baseline value at 0% strain after each loading-unloading cycle, as evident from Figure 2(a). A slight drift in the baseline is often expected in piezoresistive composites as an outcome of the irreversible slippage at the interface between the conductive graphite material and the polymer matrix.

Strain rate is another important parameter as the sensor must be able to operate for deformation at different speeds[54]. Figure 2(d) shows the sensor performance for 20% applied linear strain subjected to stretch-release cycles at different strain rates (20.5, 10.4, 3.8 and 2.3 seconds taken for each cycle). As can be noted from figure 2(d), the response is generally stable and the fluctuations in resistance variation is lower at lower strain rate as compared to higher strain rates. This can be attributed to the simultaneous reorganization of the percolation paths when the sensor is stretched and the viscoelastic relaxation of the elastomer. Hence at slower strain rate, the sensor gets enough time to stabilize the percolation path, whereas the faster actuation will be accompanied by higher chaos in the chosen percolation path. In addition to the strain rate, the gauge factor (defined as the relative change in resistance with respect to the relative change in linear dimension) is another significant metric for a strain sensor. The gauge factor was calculated (expression given in supporting information) for up to 24% linear strain and obtained result (Figure 2(e)) shows significantly high gauge factor for all operational ranges tested here. Our fabricated device showed a high gauge factor (above 100) even for very low strain values (0 to 7 %) as compared to those

values reported in literature[17, 22]. The very high values of $\Delta R/R_o$ and Gauge factor of 3854±55, attained at a strain of 24%, is 10-100 order higher than the values for strain sensors reported previously[38, 55-67] (see supplementary Table S1) with similar percolation mechanism [68, 69].

To evaluate the stability, repeatability, and predictability, the developed strain sensors were uniformly stretched to a strain value (between 0.2 to 24%, shown Figure 3) at a constant stretching rate (1mm/s) and maintained in that state for a significant amount of time (50 s) as schematically shown in **Figure 3**(a). Afterwards the sample was released at the same rate (1mm/s). (The data in Figure 3 is plotted as R/R_o instead of $\Delta R/R_o$ for better visual comparison). As shown in Figure 3(b), the relative sensor resistance variation (R/R_o) is similar for strain hold cycles of all strain values between 0.2 to 24%. When the sample is stretched, the resistance increases until the maximum strain value is reached. Further, during the holding period, the resistance value corresponding to the fixed strain is maintained as evident from the flat region. This is hugely relevant to applications such as maintaining a joint angle of a robotic hand as the sensor could provide appropriate feedback for precise control and manipulation. When the strain is released at a constant rate, the resistance decreases linearly until the initial base value is restored at zero applied strain. This is in accordance with the restoration of baseline value after each stretch-release cycle in Figure 2(a). Figure 3(c), depicting the strain hysteresis cycle of the sensor, shows some fluctuations in the instantaneous resistance at higher strain hold value as compared to the lower strain values. This can be attributed to the reconfiguration of the electrical percolation path which is more prominent at higher strain as compared to lower strain. While the strain is under hold, the resistance gradually resets to a lower value as observed from the vertical shift at the strain hold values.

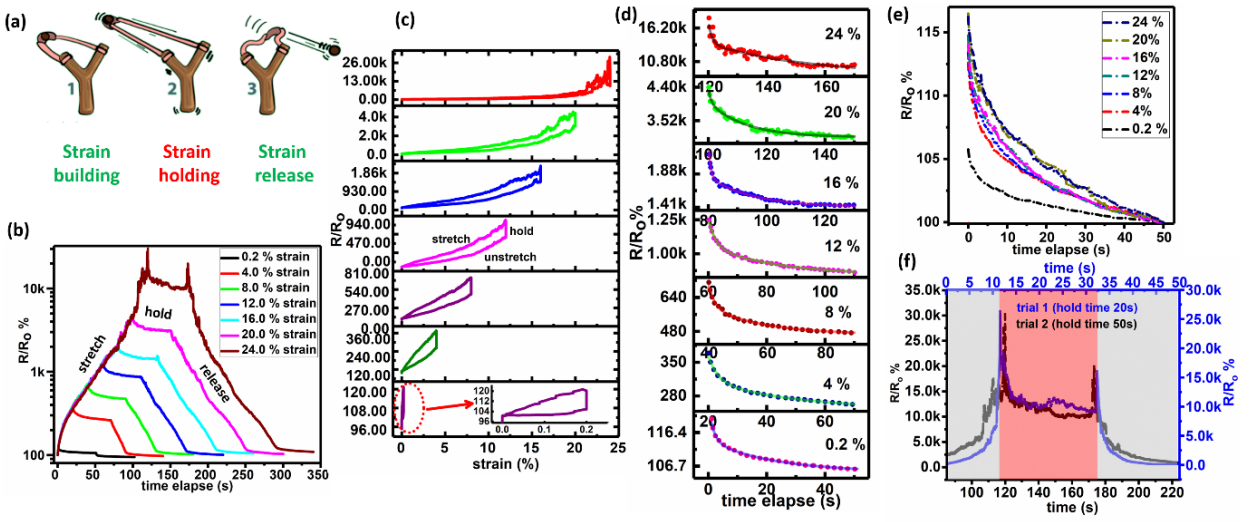

Figure. 3: (a) Strain holding characterization scheme (b) time elapsed piezoresistive response and (c) corresponding hysteresis of the sensor for stretch-release cycle response for different magnitudes of linear strain (d) The time dependent decay behaviour of the sensor during strain holding of varying magnitudes (e) The time dependent relaxation behaviour of the sensor after complete release of strain holdings (f) stretch-hold-release resistance variation as function of time for same strain values (24%) for different holding durations.

Figure 3(d) shows the time dependent variation of sensor resistance during holding at various strain values (between 0.2 to 24%). Even though the graphs in the Figure 3(b) shows a flat behaviour during the strain holding period, on a closer analysis it can be observed that the relative resistance shows an exponential relaxation decay behaviour – "self-retardation" as presented in Figure 3(d). This decay could to attributed to the system choosing the easiest available electrical percolation path [70, 71] while most of the constituent conducting particles vibrates under tension about its equilibrium position, when the sensor is undergoing the stretching. Once the stretching is stopped, the amplitude of particles vibrations slowly reduces to equilibrium state during which the percolation path constantly switches towards more and more easier paths thereby lowering the

instantaneous effective electrical resistance. The exponential decay of the piezoresistance under strain hold condition is quite similar in behaviour to the stress relaxation of the elastomeric medium during the strained state. This also asserts that the piezoresistive layer is elastically well coupled to the elastomeric substrate. Higher the strain holding, the decay curve exhibited more fluctuations from the smooth exponential relaxation since the reconfiguration of percolation path is more random and faster. Figure 3(e) shows how the sensor restores to the baseline resistance at zero strain when relaxed from various strain values. Considering the instant at which the sensor restores to initial resistance as a reference time, it can be observed that at any earlier point of time before the strain is brought to zero, the electrical resistance of the sensor decays exponentially at a rate that is dependent on the maximum strain it has experienced. For example, when the sensor is released from 24% strain, the residual stress relaxes faster (resistance decay faster as compared to that of 20% strain or other lower values). This can be attributed to the elastic stress relaxing with time and the residual stress depending on the magnitude of the strain from which the elastic medium has been restored. Figure 3(f) shows the evidence of the repeatability and reliability of the strain holding behaviour of the sensor. Here, the sensor is made to stretch upto a strain of 24% and held in that state for two different time periods (shown in primary and secondary x-axis in Figure 3(f)). The superimposed stretch-hold-release curves for the two trials reflect good consistency of the device. Also, as explained previously, piezoresistive sensors form conducting percolation network and during deformation, the conducting paths will be reorganized so that it chooses the easiest possible conducting path available at the corresponding deformed state. For lower applied strain ranges, during unloading, the original conducting paths are restored to a good proportion which will facilitate the recovery to baseline. As the applied strain goes higher, higher degree of conducting path breakage or reorganization may happen which will have more

irreversibility during unloading which creates new percolation network different from the original one. This behaviour shall also contribute to a drift in base line resistance along with other factors such as elastic behaviour of elastomer, fatigue, microcrack formations etc. In any case, the drift from baseline is attributed to several other factors and the individual contributions are not easily identified.

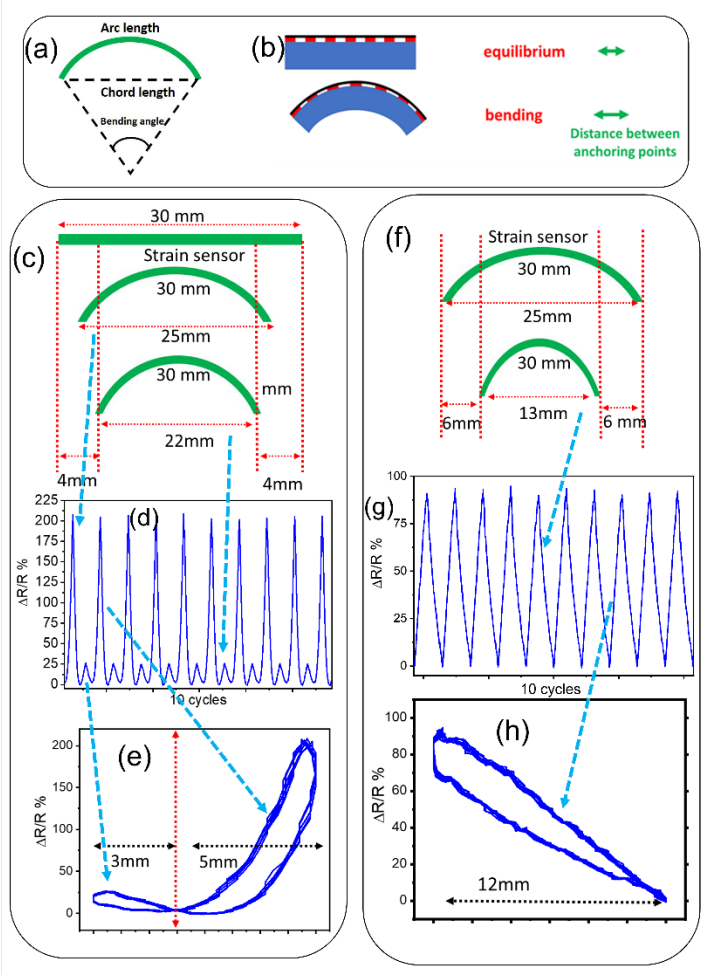

Figure. 4: (a) (b) schematic of the bending deformation of the strain sensor (c) schematic of cyclic bending from flat original state (d) corresponding relative change in resistance and (e) corresponding hysteresis cycles (f) schematic of cyclic bending from flexed state (d) corresponding relative change in resistance and (e) corresponding hysteresis cycles

The major applications of the presented strain sensors are in soft robotics which involves bending as well as stretching. Therefore, the sensor was evaluated for cyclic bending. As shown in Figure 4(a), the bending deformation can be expressed in terms of variation in chord length, similar to the bending angle. As the sample is not thin and the bending deformation may not form a perfect arc of a circle, the bending response is represented in terms of change in chord length. Initially, the sensor is mounted horizontally on the electromechanical characterisation set-up and clamped at the two ends with a deformable length of 30 mm. During the cyclic bending, the chord length varied from 30 mm to 22 mm as shown in 4 (c). Figure 4(d) shows the corresponding response of the sensor. It was observed that starting from chord length of 30 mm (up to 25 mm) the resistance decreased sharply with a relative change in the resistance of the order of 200%. Beyond chord length of 25 mm, the resistance increases and shows a variation of ~25% for the chord length variation to 22 mm. The initial decrease in resistance may be due to the sensor performing in the compression mode where the conductive graphitic particles come closer and enhance the electrical percolation. However, further bending led to tension at the interface and the graphitic layer move apart, which eventually increases the resistance. Thus, the chord length of 25 mm acts as an inversion point, about which the resistance increases with deformation in either direction. In this case, the resistance corresponding to this inversion point has been taken as the base line resistance to express $\Delta R/Ro$. This is also evident from the corresponding hysteresis given in Figure 4(e). In order to separate out the different behaviour of resistance variation, cyclic bending measurement was performed according to the schematic shown in Figure 4(f). Here, the sensor is initially maintained in the flexed state starting with a chord length of 25 mm while the deformable length remains 30 mm. Now the chord length is varied up to 13 mm and the cycles are repeated. From Figure 4(g), it can be seen that there is a monotonous increase in the resistance which is different

from the initial cyclic measurement from the unstrained flat orientation. A maximum resistance changes around 90% is obtained for the chord length variation of 13 mm from 25 mm. The corresponding hysteresis for the cyclic measurement is depicted in Figure 4(h). The magnitude of relative change in resistance during bending deformations is higher as compared to the bending performance of similar sensors reported in literature[72].

From the characterization results of the fabricated graphite paste based strain sensors, we find that the performance (average gauge factor ~ 3800) is significantly higher than most of the previous reports on piezoresistive strain sensors [68]. Moreover, the development of graphite paste showing conductivity, stretchability and sensing characteristics on flexible substrates such as Ecoflex is promising for replacing brittle copper interconnects in traditional flexible PCBs.[73] Based on various characterizations and analysis, it can be concluded that the piezoresistive behaviour of strain sensors is governed by several factors such as the supporting elastic medium, architecture of the strain sensor, materials properties, strain rate and deformation sequence, and direction. To utilize strain sensors for real scenarios in applications such as soft robotics, a proper knowledge of all these aspects is necessary. The piezoresistive strain sensors with large gauge factor and fast response need not maintain linear response in all strain ranges. Moreover, the sensors performance may be influenced by environmental factors such as temperature variations, uneven surfaces, and electric potential fluctuations. All these parameters are measurable, accountable, and predictable. For example, as discussed in previous sections, the hysteresis behaviour is repeatable and from the hysteresis patterns, the origin (e.g., from bending or stretching or twisting) could be distinguished. Thus, depending on the application, the hysteresis in the cyclic loading-release strain may be acceptable. Even the time dependent relaxation of the piezoresistance under constant strain is predicable with mathematical functions. In fact, the

hysteresis and relaxation behaviour of the sensor is associated with the viscoelastic properties of the supporting elastomer matrix and hence it is not completely avoidable and is a sign of well couped sensor and the support matrix. Hence instead of attempting to develop perfectly linear and low hysteresis piezoresistive strain sensors, it may be more efficient to predict the non-linear behaviour of the sensor. In this regard, use of machine learning [74] and artificial intelligence [75] could also be useful.

3. Conclusion

In summary, the custom graphite paste based elastomeric strain sensor with Velcro enabled macro-features, exhibits excellent performance (sensitivity ~ 16500 % and gauge factor ~ 3800) along with excellent flexibility, stretchability, and repeatability. The comparison of our device with previously reported stretchable sensors shows the best gauge factor even at lower stretchable ranges. The sensing performance at varying linear stretching shows proportional increase in the sensitivity. The sensor response at different strain rates demonstrate its suitability for diverse applications with complex deformations. The viscoelastic hysteresis behaviour which is a typical of piezoresistive strain sensors has been investigated to understand the reliability of the design and functionality. The strain holding experiments provide good insights into the viscoelastic relaxation behaviour of piezoresistive systems. The evaluation of the presented strain sensor at bending and stretching allows identification of complex deformation and equilibrium states by real-time feedback from the strain sensors when employed in robotics and other mechanical applications. These investigations assert the need for greater focus on understanding the parameters influencing the piezoresistive sensing behaviour so that complex dynamics of the mechanical systems could be interpreted instead of the absolute strain values alone.

Experimental Methods

***Sensor Fabrication*:** The fabrication of strain sensor using graphite paste as sensing material and Ecoflex™ 00-30 as substrate is carried out in four major steps as shown in supporting information Figure 1 (a) and (b). For graphite paste preparation, in step (i) 2 wt.% of dispersant Triton X-100 (Sigma Aldrich) was dissolved in a solvent terpineol (Sigma Aldrich). Following this, (ii) the binder ethyl cellulose (5 wt.%, sigma Aldrich) was added and stirred continuously for 2 hrs. to get homogeneous solution. Finally, graphite powder was added to the binder solution and stirred overnight (12 hrs.) to obtain a homogenous printable paste (the properties including viscosity details are given in supporting information). In step (ii) the elastomeric substrate of the strain sensor is also designed to print the graphite paste. For this the Part A and Part B components of commercial Ecoflex™ 00-30 are taken in equal ratio and mixed thoroughly. Afterwards, in step (iii) the mixture is poured as a thin layer on a rectangular flat surface over contour of 5.5 cm x 2.5 cm defined with a commercially available Velcro tape. Once the elastomer is cured, it is peeled off from the Velcro tape with the Velcro features engraved on the lower surface of the elastomer. Now the elastomer layer is turned and placed upside down so that the patterned surface is on the top surface. In step (iv) a uniform thin layer of the formulated graphite paste is applied on the defined sensor area (4.5 cm x 1 cm) on the surface of the elastomer with the imprinted Velcro hook structured pores. Further, the sample is dried in an oven at a temperature of 50ºC until the solvent of the graphite paste is completely evaporated. Following this, electrical contacts are realized on the sample with fine copper wires and silver paste and a local encapsulation is made at the contact point with epoxy. In the final step (v), another thin layer of Ecoflex is uniformed spread over the elastomer layer and cured to obtain seamlessly integrated sensor within the elastomer. This

arrangement also prevents the potential physical damage to the sensor material from external impacts. The characterization set-up of the strain sensor is given in supporting information.

Graphite Paste formation and properties: In the graphite paste, the Triton X-100 act as surfactant to stabilize the graphite particle in the suspension. The purpose of the terpineol is to act as a medium to control the flow of the ink and to suspend the particles for better homogeneity in the printed pattern. Ethyl cellulose serves as binders for the graphite sensing material and mediates the anchoring of the sensing layers on the elastomer. These anchor points serve as nodes about which the percolation paths for the electrical conduction can vary systematically with respect to the dimensional changes of the elastomer by external mechanical strains thereby forming a piezoresistive strain sensor. The viscosity analysis of the formulated paste was performed using a viscometer (Cole Parmer, Serial: VCPL 450015; P/N98965-49) and the result is given in Figure S1.(a). The typical shear thinning behaviour was observed for the formulated paste. This shear thinning behaviour is one of the prerequisites for a paste to form better printed pattern.

Supporting Information.

Figure. S1. Graphical representation of performance metrics (gauge factor and stretchability) of state-of-art strain sensors.

Figure. S2. (a) image of strain sensor in the linear stretching arrangement on custom experimental set-up. (b) schematic of the Velcro enabled strain sensor design and anchoring effect (c) SEM micrograph of graphite paste layer on the substrate.

Figure. S3: (a)-(c) optical microscopic image of the Ecoflex layer with Velcro structured patterning (g) (h) schematic of the in-plane deformations of the ecoflex layer with engraved velcro features (i) photograph of velcro tape used for device fabrication (j) schematic of the in-plane deformation of a single velcro hook structure engraved in Ecoflex.

Table S1. Comparison of present work with the performance of other piezoresistive carbonous-polymer strain sensors based on the values obtained from literatures.

AUTHOR INFORMATION

Corresponding Author

*Ravinder Dahiya**

E-mail: Ravinder.Dahiya@glasgow.ac.uk.

Author Contributions

The manuscript was written through contributions of all authors. All authors have given approval to the final version of the manuscript.

Funding Sources

This work was supported in part by the Engineering and Physical Sciences Research Council (EPSRC) through Engineering Fellowship for Growth (EP/R029644/1) and European Commission through Marie Sklodowska-Curie Actions International Fellowship (H2020-MSCA-IF-2017-798639).

ACKNOWLEDGMENT

This work was supported in part by the Engineering and Physical Sciences Research Council (EPSRC) through Engineering Fellowship for Growth (EP/R029644/1) and European Commission through Marie Sklodowska-Curie Actions International Fellowship (H2020-MSCA-IF-2017-798639).

References

1. Liao, X.; Zhang, Z.; Liao, Q.; Liang, Q.; Ou, Y.; Xu, M.; Li, M.; Zhang, G.; Zhang, Y., Flexible and printable paper-based strain sensors for wearable and large-area green electronics. *Nanoscale* **2016,** *8* (26), 13025-13032.

2. Dahiya, R. S.; Valle, M., *Robotic tactile sensing: technologies and system*. Springer Science & Business Media: 2013.
3. Kumaresan, Y.; Kim, H.; Pak, Y.; Poola, P. K.; Lee, R.; Lim, N.; Ko, H. C.; Jung, G. Y.; Dahiya, R., Omnidirectional Stretchable inorganic‐material‐based electronics with enhanced performance. *Advanced Electronic Materials* **2020,** *6* (7), 2000058.
4. Dubey, P. K.; Yogeswaran, N.; Liu, F.; Vilouras, A.; Kaushik, B. K.; Dahiya, R., Monolayer $MoSe_2$-Based Tunneling Field Effect Transistor for Ultrasensitive Strain Sensing. *IEEE Transactions on Electron Devices* **2020,** *67* (5), 2140-2146.
5. Gao, W.; Ota, H.; Kiriya, D.; Takei, K.; Javey, A., Flexible electronics toward wearable sensing. *Accounts of chemical research* **2019,** *52* (3), 523-533.
6. Liao, X.; Zhang, Z.; Kang, Z.; Gao, F.; Liao, Q.; Zhang, Y., Ultrasensitive and stretchable resistive strain sensors designed for wearable electronics. *Materials Horizons* **2017,** *4* (3), 502-510.
7. Sencadas, V.; Mutlu, R.; Alici, G., Large area and ultra-thin compliant strain sensors for prosthetic devices. *Sensors and Actuators A: Physical* **2017,** *266*, 56-64.
8. Bhattacharjee, M.; Soni, M.; Escobedo, P.; Dahiya, R., PEDOT: PSS Microchannel‐Based Highly Sensitive Stretchable Strain Sensor. *Advanced Electronic Materials* **2020,** *6* (8), 2000445.
9. Zhang, Y.; Anderson, N.; Bland, S.; Nutt, S.; Jursich, G.; Joshi, S., All-printed strain sensors: Building blocks of the aircraft structural health monitoring system. *Sensors and Actuators A: Physical* **2017,** *253*, 165-172.
10. Lee, G.-Y.; Kim, M.-S.; Yoon, H.-S.; Yang, J.; Ihn, J.-B.; Ahn, S.-H., Direct printing of strain sensors via nanoparticle printer for the applications to composite structural health monitoring. *Procedia CIRP* **2017,** *66*, 238-242.
11. Nikbakhtnasrabadi, F.; El Matbouly, H.; Ntagios, M.; Dahiya, R., Textile-Based Stretchable Microstrip Antenna with Intrinsic Strain Sensing. *ACS Applied Electronic Materials* **2021,** *3* (5), 2233-2246.
12. Amjadi, M.; Kyung, K. U.; Park, I.; Sitti, M., Stretchable, skin‐mountable, and wearable strain sensors and their potential applications: a review. *Advanced Functional Materials* **2016,** *26* (11), 1678-1698.
13. Wang, Y.; Wang, L.; Yang, T.; Li, X.; Zang, X.; Zhu, M.; Wang, K.; Wu, D.; Zhu, H., Wearable and highly sensitive graphene strain sensors for human motion monitoring. *Advanced Functional Materials* **2014,** *24* (29), 4666-4670.
14. Cheng, S.; Narang, Y. S.; Yang, C.; Suo, Z.; Howe, R. D., Stick‐on large‐strain sensors for soft robots. *Advanced Materials Interfaces* **2019,** *6* (20), 1900985.
15. Prakash Karipoth, A. Christou, Abhilash Pullanchiyodan, Ravinder Dahiya, Bioinspired Inchworm and Earthworm like Soft Robots with Intrinsic Strain Sensing. *Advanced Intelligent Systems,* 2100092*,* **2021**.
16. Ozioko, O.; Karipoth, P.; Escobedo, P.; Ntagios, M.; Pullanchiyodan, A.; Dahiya, R., SensAct: The Soft and Squishy Tactile Sensor with Integrated Flexible Actuator. *Advanced Intelligent Systems* **2021,** *3* (3), 1900145.
17. Duan, L.; D'hooge, D. R.; Cardon, L., Recent progress on flexible and stretchable piezoresistive strain sensors: from design to application. *Progress in Materials Science* **2020,** *114*, 100617.

18. Atalay, A.; Sanchez, V.; Atalay, O.; Vogt, D. M.; Haufe, F.; Wood, R. J.; Walsh, C. J., Batch fabrication of customizable silicone‐textile composite capacitive strain sensors for human motion tracking. *Advanced Materials Technologies* **2017,** *2* (9), 1700136.
19. Georgopoulou, A.; Clemens, F., Piezoresistive Elastomer-Based Composite Strain Sensors and Their Applications. *ACS Applied Electronic Materials* **2020,** *2* (7), 1826-1842.
20. Tavassolian, M.; Cuthbert, T. J.; Napier, C.; Peng, J.; Menon, C., Textile‐Based Inductive Soft Strain Sensors for Fast Frequency Movement and Their Application in Wearable Devices Measuring Multiaxial Hip Joint Angles during Running. *Advanced Intelligent Systems* **2020,** *2* (4), 1900165.
21. Kamita, G.; Frka‐Petesic, B.; Allard, A.; Dargaud, M.; King, K.; Dumanli, A. G.; Vignolini, S., Biocompatible and Sustainable Optical Strain Sensors for Large‐Area Applications. *Advanced Optical Materials* **2016,** *4* (12), 1950-1954.
22. Souri, H.; Banerjee, H.; Jusufi, A.; Radacsi, N.; Stokes, A. A.; Park, I.; Sitti, M.; Amjadi, M., Wearable and stretchable strain sensors: materials, sensing mechanisms, and applications. *Advanced Intelligent Systems* **2020,** *2* (8), 2000039.
23. Amjadi, M.; Pichitpajongkit, A.; Lee, S.; Ryu, S.; Park, I., Highly stretchable and sensitive strain sensor based on silver nanowire–elastomer nanocomposite. *ACS nano* **2014,** *8* (5), 5154-5163.
24. Chen, Q.; Sun, Y.; Wang, Y.; Cheng, H.; Wang, Q.-M., ZnO nanowires–polyimide nanocomposite piezoresistive strain sensor. *Sensors and Actuators A: Physical* **2013,** *190*, 161-167.
25. Chossat, J.-B.; Park, Y.-L.; Wood, R. J.; Duchaine, V., A soft strain sensor based on ionic and metal liquids. *Ieee sensors journal* **2013,** *13* (9), 3405-3414.
26. Zhai, W.; Xia, Q.; Zhou, K.; Yue, X.; Ren, M.; Zheng, G.; Dai, K.; Liu, C.; Shen, C., Multifunctional flexible carbon black/polydimethylsiloxane piezoresistive sensor with ultrahigh linear range, excellent durability and oil/water separation capability. *Chemical Engineering Journal* **2019,** *372*, 373-382.
27. Li, W.; Guo, J.; Fan, D., 3D graphite–polymer flexible strain sensors with Ultrasensitivity and durability for real‐time human vital sign monitoring and musical instrument education. *Advanced Materials Technologies* **2017,** *2* (6), 1700070.
28. Lee, S. W.; Park, J. J.; Park, B. H.; Mun, S. C.; Park, Y. T.; Liao, K.; Seo, T. S.; Hyun, W. J.; Park, O. O., Enhanced sensitivity of patterned graphene strain sensors used for monitoring subtle human body motions. *ACS applied materials & interfaces* **2017,** *9* (12), 11176-11183.
29. Gao, Y.; Fang, X.; Tan, J.; Lu, T.; Pan, L.; Xuan, F., Highly sensitive strain sensors based on fragmentized carbon nanotube/polydimethylsiloxane composites. *Nanotechnology* **2018,** *29* (23), 235501.
30. Shi, X.; Wang, H.; Xie, X.; Xue, Q.; Zhang, J.; Kang, S.; Wang, C.; Liang, J.; Chen, Y., Bioinspired ultrasensitive and stretchable MXene-based strain sensor via nacre-mimetic microscale "brick-and-mortar" architecture. *ACS nano* **2018,** *13* (1), 649-659.
31. Zhang, C.; Li, H.; Huang, A.; Zhang, Q.; Rui, K.; Lin, H.; Sun, G.; Zhu, J.; Peng, H.; Huang, W., Rational Design of a Flexible CNTs@ PDMS Film Patterned by Bio‐Inspired Templates as a Strain Sensor and Supercapacitor. *Small* **2019,** *15* (18), 1805493.
32. Beker, L.; Matsuhisa, N.; You, I.; Ruth, S. R. A.; Niu, S.; Foudeh, A.; Tok, J. B.-H.; Chen, X.; Bao, Z., A bioinspired stretchable membrane-based compliance sensor. *Proceedings of the National Academy of Sciences* **2020,** *117* (21), 11314-11320.

33. Yin, B.; Liu, X.; Gao, H.; Fu, T.; Yao, J., Bioinspired and bristled microparticles for ultrasensitive pressure and strain sensors. *Nature communications* **2018,** *9* (1), 1-8.
34. Escobedo, P.; Bhattacharjee, M.; Nikbakhtnasrabadi, F.; Dahiya, R., Smart Bandage with Wireless Strain and Temperature Sensors and Battery-less NFC Tag. *IEEE Internet of Things Journal,* Vol 8(6), pp 5093-5100, **2021**.
35. Dahiya, R.; Yogeswaran, N.; Liu, F.; Manjakkal, L.; Burdet, E.; Hayward, V.; Jörntell, H., Large-area soft e-skin: The challenges beyond sensor designs. *Proceedings of the IEEE* **2019,** *107* (10), 2016-2033.
36. Zhao, J.; Chi, Z.; Yang, Z.; Chen, X.; Arnold, M. S.; Zhang, Y.; Xu, J.; Chi, Z.; Aldred, M. P., Recent developments of truly stretchable thin film electronic and optoelectronic devices. *Nanoscale* **2018,** *10* (13), 5764-5792.
37. Liu, Y.; Pharr, M.; Salvatore, G. A., Lab-on-skin: a review of flexible and stretchable electronics for wearable health monitoring. *ACS nano* **2017,** *11* (10), 9614-9635.
38. Zhou, Y.; Zhan, P.; Ren, M.; Zheng, G.; Dai, K.; Mi, L.; Liu, C.; Shen, C., Significant stretchability enhancement of a crack-based strain sensor combined with high sensitivity and superior durability for motion monitoring. *ACS applied materials & interfaces* **2019,** *11* (7), 7405-7414.
39. Araromi, O. A.; Graule, M. A.; Dorsey, K. L.; Castellanos, S.; Foster, J. R.; Hsu, W.-H.; Passy, A. E.; Vlassak, J. J.; Weaver, J. C.; Walsh, C. J., Ultra-sensitive and resilient compliant strain gauges for soft machines. *Nature* **2020,** *587* (7833), 219-224.
40. Fu, X.; Ramos, M.; Al-Jumaily, A. M.; Meshkinzar, A.; Huang, X., Stretchable strain sensor facilely fabricated based on multi-wall carbon nanotube composites with excellent performance. *Journal of Materials Science* **2019,** *54* (3), 2170-2180.
41. Narongthong, J.; Wießner, S.; Hait, S.; Sirisinha, C.; Stöckelhuber, K. W., Strain-rate independent small-strain-sensor: enhanced responsiveness of carbon black filled conductive rubber composites at slow deformation by using an ionic liquid. *Composites Science and Technology* **2020,** *188*, 107972.
42. Choi, D. Y.; Kim, M. H.; Oh, Y. S.; Jung, S.-H.; Jung, J. H.; Sung, H. J.; Lee, H. W.; Lee, H. M., Highly stretchable, hysteresis-free ionic liquid-based strain sensor for precise human motion monitoring. *ACS applied materials & interfaces* **2017,** *9* (2), 1770-1780.
43. Kim, K. K.; Hong, S.; Cho, H. M.; Lee, J.; Suh, Y. D.; Ham, J.; Ko, S. H., Highly sensitive and stretchable multidimensional strain sensor with prestrained anisotropic metal nanowire percolation networks. *Nano letters* **2015,** *15* (8), 5240-5247.
44. Oliveri, A.; Maselli, M.; Lodi, M.; Storace, M.; Cianchetti, M., Model-based compensation of rate-dependent hysteresis in a piezoresistive strain sensor. *IEEE Transactions on Industrial Electronics* **2018,** *66* (10), 8205-8213.
45. Sanchez, C.; Arribart, H.; Guille, M. M. G., Biomimetism and bioinspiration as tools for the design of innovative materials and systems. *Nature materials* **2005,** *4* (4), 277-288.
46. Liu, J.; Zhao, F.; Tao, Q.; Cao, J.; Yu, Y.; Zhang, X., Visualized simulation for the nanostructure design of flexible strain sensors: from a numerical model to experimental verification. *Materials Horizons* **2019,** *6* (9), 1892-1898.
47. Zhu, J.; Wan, C.; Xu, H.; Liu, Y.; Zhuang, J.; Sun, J.; Gao, X.; McNally, T.; Huang, Y.; Wu, D., An anchoring array assembly method for enhancing the electrical conductivity of composites of polypropylene and hybrid fillers. *Composites Science and Technology* **2021,** *211*, 108846.

48. Zhu, G.-J.; Ren, P.-G.; Guo, H.; Jin, Y.-L.; Yan, D.-X.; Li, Z.-M., Highly sensitive and stretchable polyurethane fiber strain sensors with embedded silver nanowires. *ACS applied materials & interfaces* **2019,** *11* (26), 23649-23658.
49. Hannigan, B. C.; Cuthbert, T. J.; Geng, W.; Tavassolian, M.; Menon, C., Understanding the Impact of Machine Learning Models on the Performance of Different Flexible Strain Sensor Modalities. *Frontiers in Materials* **2021,** *8*, 44.
50. Cantournet, S.; Desmorat, R.; Besson, J., Mullins effect and cyclic stress softening of filled elastomers by internal sliding and friction thermodynamics model. *International Journal of Solids and Structures* **2009,** *46* (11-12), 2255-2264.
51. Min, S. H.; Asrulnizam, A.; Atsunori, M.; Mariatti, M., Properties of Stretchable and Flexible Strain Sensor Based on Silver/PDMS Nanocomposites. *Materials Today: Proceedings* **2019,** *17*, 616-622.
52. Zhang, Y.; Li, M.; Han, X.; Fan, Z.; Zhang, H.; Li, Q., High-strength and highly electrically conductive hydrogels for wearable strain sensor. *Chemical Physics Letters* **2021,** *769*, 138437.
53. Haghgoo, M.; Hassanzadeh-Aghdam, M.; Ansari, R., A comprehensive evaluation of piezoresistive response and percolation behavior of multiscale polymer-based nanocomposites. *Composites Part A: Applied Science and Manufacturing* **2020,** *130*, 105735.
54. Moriche, R.; Jiménez-Suárez, A.; Sánchez, M.; Prolongo, S.; Ureña, A., Sensitivity, influence of the strain rate and reversibility of GNPs based multiscale composite materials for high sensitive strain sensors. *Composites Science and Technology* **2018,** *155*, 100-107.
55. Wang, Y.; Hao, J.; Huang, Z.; Zheng, G.; Dai, K.; Liu, C.; Shen, C., Flexible electrically resistive-type strain sensors based on reduced graphene oxide-decorated electrospun polymer fibrous mats for human motion monitoring. *Carbon* **2018,** *126*, 360-371.
56. Xu, M.; Qi, J.; Li, F.; Zhang, Y., Highly stretchable strain sensors with reduced graphene oxide sensing liquids for wearable electronics. *Nanoscale* **2018,** *10* (11), 5264-5271.
57. Wu, S.; Peng, S.; Han, Z. J.; Zhu, H.; Wang, C. H., Ultrasensitive and stretchable strain sensors based on mazelike vertical graphene network. *ACS applied materials & interfaces* **2018,** *10* (42), 36312-36322.
58. Guo, X.; Huang, Y.; Zhao, Y.; Mao, L.; Gao, L.; Pan, W.; Zhang, Y.; Liu, P., Highly stretchable strain sensor based on SWCNTs/CB synergistic conductive network for wearable human-activity monitoring and recognition. *Smart Materials and Structures* **2017,** *26* (9), 095017.
59. Zhang, F.; Wu, S.; Peng, S.; Sha, Z.; Wang, C. H., Synergism of binary carbon nanofibres and graphene nanoplates in improving sensitivity and stability of stretchable strain sensors. *Composites Science and Technology* **2019,** *172*, 7-16.
60. Tang, Z.; Jia, S.; Wang, F.; Bian, C.; Chen, Y.; Wang, Y.; Li, B., Highly stretchable core–sheath fibers via wet-spinning for wearable strain sensors. *ACS applied materials & interfaces* **2018,** *10* (7), 6624-6635.
61. Han, F.; Li, J.; Zhao, S.; Zhang, Y.; Huang, W.; Zhang, G.; Sun, R.; Wong, C.-P., A crack-based nickel@ graphene-wrapped polyurethane sponge ternary hybrid obtained by electrodeposition for highly sensitive wearable strain sensors. *Journal of Materials Chemistry C* **2017,** *5* (39), 10167-10175.
62. Huang, Y.; Zhao, Y.; Wang, Y.; Guo, X.; Zhang, Y.; Liu, P.; Liu, C.; Zhang, Y., Highly stretchable strain sensor based on polyurethane substrate using hydrogen bond-assisted

laminated structure for monitoring of tiny human motions. *Smart Materials and Structures* **2018,** *27* (3), 035013.
63. Wang, Y.; Jia, Y.; Zhou, Y.; Wang, Y.; Zheng, G.; Dai, K.; Liu, C.; Shen, C., Ultra-stretchable, sensitive and durable strain sensors based on polydopamine encapsulated carbon nanotubes/elastic bands. *Journal of Materials Chemistry C* **2018,** *6* (30), 8160-8170.
64. Wang, X.; Sun, H.; Yue, X.; Yu, Y.; Zheng, G.; Dai, K.; Liu, C.; Shen, C., A highly stretchable carbon nanotubes/thermoplastic polyurethane fiber-shaped strain sensor with porous structure for human motion monitoring. *Composites Science and Technology* **2018,** *168*, 126-132.
65. Ren, J.; Du, X.; Zhang, W.; Xu, M., From wheat bran derived carbonaceous materials to a highly stretchable and durable strain sensor. *RSC advances* **2017,** *7* (37), 22619-22626.
66. Li, G.; Dai, K.; Ren, M.; Wang, Y.; Zheng, G.; Liu, C.; Shen, C., Aligned flexible conductive fibrous networks for highly sensitive, ultrastretchable and wearable strain sensors. *Journal of Materials Chemistry C* **2018,** *6* (24), 6575-6583.
67. Ma, J.; Wang, P.; Chen, H.; Bao, S.; Chen, W.; Lu, H., Highly sensitive and large-range strain sensor with a self-compensated two-order structure for human motion detection. *ACS applied materials & interfaces* **2019,** *11* (8), 8527-8536.
68. Duan, L.; D'hooge, D. R.; Cardon, L., Recent progress on flexible and stretchable piezoresistive strain sensors: from design to application. *Progress in Materials Science* **2019**, 100617.
69. Huang, X.; Yin, Z.; Wu, H., Structural Engineering for High‐Performance Flexible and Stretchable Strain Sensors. *Advanced Intelligent Systems*, 2000194.
70. Hu, N.; Karube, Y.; Yan, C.; Masuda, Z.; Fukunaga, H., Tunneling effect in a polymer/carbon nanotube nanocomposite strain sensor. *Acta materialia* **2008,** *56* (13), 2929-2936.
71. Hwang, H.; Kim, Y.; Park, J. H.; Jeong, U., 2D Percolation Design with Conductive Microparticles for Low‐Strain Detection in a Stretchable Sensor. *Advanced Functional Materials* **2020,** *30* (13), 1908514.
72. Amjadi, M.; Turan, M.; Clementson, C. P.; Sitti, M., Parallel microcracks-based ultrasensitive and highly stretchable strain sensors. *ACS applied materials & interfaces* **2016,** *8* (8), 5618-5626.
73. Christoe, M. J.; Han, J.; Kalantar‐Zadeh, K., Telecommunications and data processing in flexible electronic systems. *Advanced Materials Technologies* **2020,** *5* (1), 1900733.
74. Gholami, M.; Ejupi, A.; Rezaei, A.; Ferrone, A.; Menon, C. In *Estimation of knee joint angle using a fabric-based strain sensor and machine learning: A preliminary investigation*, 2018 7th IEEE International Conference on Biomedical Robotics and Biomechatronics (Biorob), IEEE: 2018; pp 589-594.
75. Oldfrey, B.; Jackson, R.; Smitham, P.; Miodownik, M., A Deep Learning Approach to Non-linearity in Wearable Stretch Sensors. *Front. Robot. AI 6: 27. doi: 10.3389/frobt* **2019**.

Table of Content

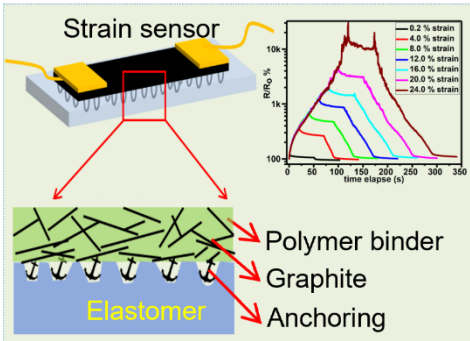

TOC figure only